Electronic Supporting Information

Fe$_6$Ge$_5$—formation and collapse of a core-shell structure during the oxygen evolution reaction

J. Niklas Hausmann,[a] Roman A. Khalaniya,[b] Chittaranjan Das,[c] Ina Remy-Speckmann,[a] Stefan Berendts,[a] Andrei V. Shevelkov,[b] Matthias Driess*[a] and Prashanth W. Menezes*[a]

[a] Department of Chemistry, Technische Universität Berlin, Straße des 17 Juni 135, Sekr. C2, 10623 Berlin, Germany.
*E-mail: matthias.driess@tu-berlin.de; prashanth.menezes@mailbox.tu-berlin.de

[b] Department of Chemistry, Lomonosov Moscow State University, 119991 Moscow, Russia

[c] Karlsruhe Institute of Technology (KIT), Institute for Applied Materials (IAM-ESS), Hermann-von-Helmholtz-Platz 1, D-76344 Eggenstein-Leopoldshafen.

Experimental

Synthesis of Fe₆Ge₅. Fe powder (Sigma Aldrich, 99.99%) and Ge chips (Sigma Aldrich, 99.999%) were used as starting materials. The elements, taken in a 6:5 ratio, were sealed into an evacuated quartz ampoule and annealed at 1273 K for 2 days. Afterwards, the sample was ground in an agate mortar, pressed into a pellet 8 mm in diameter, and annealed again in a sealed and evacuated quartz ampoule at 923 K for 7 days.

Synthesis of the reference materials: The synthesis of the reference materials is described in B. Chakraborty, *et al.* and J. N. Hausmann *et al.*[1,2]

Electrochemical measurements

All measurements were performed with a thermostat at 25 °C. A standard three-electrode (working, counter and reference) electrochemical cell with 50 ml 1 M aqueous KOH (Alfa Aesar 1.0 N standardized solution) and a potentiostat (SP-200, BioLogic Science Instruments) controlled by the EC-Lab v10.20 software package was used for the investigations. Fluorine-doped tin oxide (FTO) glass plates (2 × 1 cm²) with deposited sample (0.4 mg, 1 × 1 cm²) or nickel foam (NF) with deposited sample (1 mg, 1 × 1 cm²) served as working electrodes, Pt wire (0.5 mm diameter × 230 mm length; A-002234, BioLogic) as counter and Hg/HgO as the reference electrode (CH Instruments, Inc.). Electrochemical data was measured with three different samples and then data of a representative sample shown.

Electrophoretic deposition (EPD). The materials were deposited electrophoretically by a well-established method on FTO and NF.[3–6] In a mixture of iodine, acetone, and mortar grounded sample (e.g. Fe₆Ge₅), a potential of 10 V against open circuit potential was applied. Either two FTO or two NF were used as counter and reference electrode and an area of 1 × 1 cm² was inside of the solution. Through keto-enol tautomerisation, acetone and iodine produces protons. These formed protons are adsorbed on the surface of the suspended particles (e.g. Fe₆Ge₅) and create a positive surface charge. Due to the applied electric field, the charged particles migrate towards the cathode where they deposit. Usually, 25 mg of mortar grounded catalyst powder was added to 8 ml acetone and sonicated at room temperature for 2 h. Subsequently, 2 mg I₂ was added, and the suspension sonicated for another 3 min. Then the EPD was performed under stirring at 10 V for 1-10 min to obtain uniform films. The sample loading was determined by weighting the electrodes before and after the process. The EPD time was adjusted in a way that the desired loading, 0.4 mg/cm² on FTO and 1 mg/cm² on NF, was obtained for all presented materials.

***iR* compensation:** The uncompensated resistance (R_u) was determined by impedance spectroscopy at 100 MHz and a potential of 1.175 V_{RHE} with an amplitude of 10 mV prior to the measurements and usually

found to be in the range of 10-12 Ω for FTO and 1-1.4 Ω for NF. The potential was then corrected by 90% of R_u by the potentiostat during the measurement.

Linear scan voltammetry (LSV). LSV was performed without stirring and with *iR* compensation. We never show the first LSV but the second, or if the material activated, the first stable LSV. For Fe_6Ge_5 we showed the second LSV. The potentials were referenced to the reversible hydrogen electrode (V_{RHE}), and in 1 M aqueous KOH (pH 13.8) the potential was calculated using the following equation:

$$E(RHE) = E(Hg/HgO) + 0.098 \text{ V} + (0.059 \times pH) \text{ V}.$$

Chronoamperometry (CA). The CA measurements were performed under strong stirring and an *iR* compensation of 90%.

Steady state Tafel analysis. CA measurements for 3 min at each potential were performed to obtain the respective current density (i). Then, the Tafel slope was calculated according to the Tafel equation, $\eta = b \times \log(i) + a$, where η is the overpotential, b is the Tafel slope, i is the current density, and a is a variable proportional to the logarithm of the exchange current density.

Double-layer capacitance (C_{dl}). The C_{dl} was determined from CVs cycled between 0.736 and 0.786 V_{RHE}, where no apparent Faradaic process occurred. Half of the potential difference at 0.761 V_{RHE} was plotted against the scan rate, and, by linear regression, a slope was obtained which is the C_{dl}.[7,8]

Electrochemical impedance spectroscopy (EIS). EIS was recorded at 1.50 $V_{RHE.}$ Using an amplitude of 10 mV, the sinusoidal wave was examined in the frequency range 100 kHz to 1 mHz. From the diameter of the semicircle in the Nyquist plots, the charge-transfer resistance (R_{ct}) was approximated.[7]

Faradaic efficiency (FE). The FE of Fe_6Ge_5 in 1 M KOH towards the oxygen evolution reaction (OER) was determined in a two-electrode configuration where Fe_6Ge_5/NF was used as anode and Pt wire as a cathode. A constant current of 100 mA/cm² was applied for 45 min. The respective oxygen and hydrogen gas voluminal were collected and measured at four different times (see Fig. S12 for the setup). First, the Faradaic efficiency can be calculated on the respective gas volume of O_2 and H_2 (100% FE for a ratio of 1 to 2). Second, to relate the current, Q, to the gas volume, V, we used the ideal gas law, $n = (pV)/(RT)$, where n is the amount of gas molecules, p the pressure, R the ideal gas constant, and T the temperature. Using the relation $n = (It)/4F$, where I is the current, t the time, and F the Faraday constant, we compared the expected volume of O_2 with the one measured.

Characterization details

Powder X-ray diffraction (pXRD). A Panalytical X'Pert PRO diffractometer and a Rigaku SmartLab 3 kW diffractometer (both in Bragg-Brentano geometry, Cu-K$_\alpha$ radiation 1.54184 Å) were used for pXRD measurements.

X-ray photoelectron spectroscopy (XPS). The XPS measurements were done using ThermoFischer's Escalab 250 spectrometer. The samples were excited with monochromatic Al-kα excitation (1486.6 eV), and the photo emitted electrons were collected at the concentric hemispherical analyser with a pass energy of 10 eV spectrometer. A magnetic collector lens was used to collect the maximum of photo emitted electrons to the analyser. The analysis was done using Avantage software from Thermo Fischer.

Scanning electron microscopy (SEM). SEM was performed on a GeminiSEM500 NanoVP microscope (ZEISS) integrated with an energy dispersive X-ray (EDX) detector (Bruker Quantax XFlash® 6|60). The software package EDAX was used for data handling and analysis. The SEM experiments were performed at the Zentrum für Elektronenmikroskopie (ZELMI) of the TU Berlin.

Transmission electron microscopy (TEM). TEM was conducted on an FEI Tecnai G2 20 S-TWIN transmission electron microscope (FEI Company, Eindhoven, Netherlands) equipped with a LaB$_6$ source at 200 kV acceleration voltage. The films were scratched off from the FTO substrate and transferred onto a carbon-coated copper grid for their investigation after catalysis. EDX analyses were achieved with an EDAX r-TEM SUTW detector (Si (Li) detector). A GATAN MS794 P CCD camera was used to collect the images. The TEM experiments were conducted at the Zentrum für Elektronenmikroskopie (ZELMI) of the TU Berlin.

Atom	Ox.	Wyck.	Site	x/a	y/b	z/c
Fe1	0	4i	m	0.1229(4)	0	0.0153(5)
Fe2	0	4f	-1	1/4	1/4	1/2
Fe3	0	4h	2	0	0.2533(4)	1/2
Fe4	0	8j	1	0.2846(6)	0.2605(4)	0.1755(5)
Fe5	0	4i	m	0.0793(5)	1/2	0.2806(6)
Ge1	0	4i	m	0.3645(3)	0	0.0068(3)
Ge2	0	8j	1	0.0451(3)	0.1970(6)	0.2125(3)
Ge3	0	4i	m	0.3420(4)	0	0.3720(5)
Ge4	0	4i	m	0.3515(4)	1/2	0.4000(5)
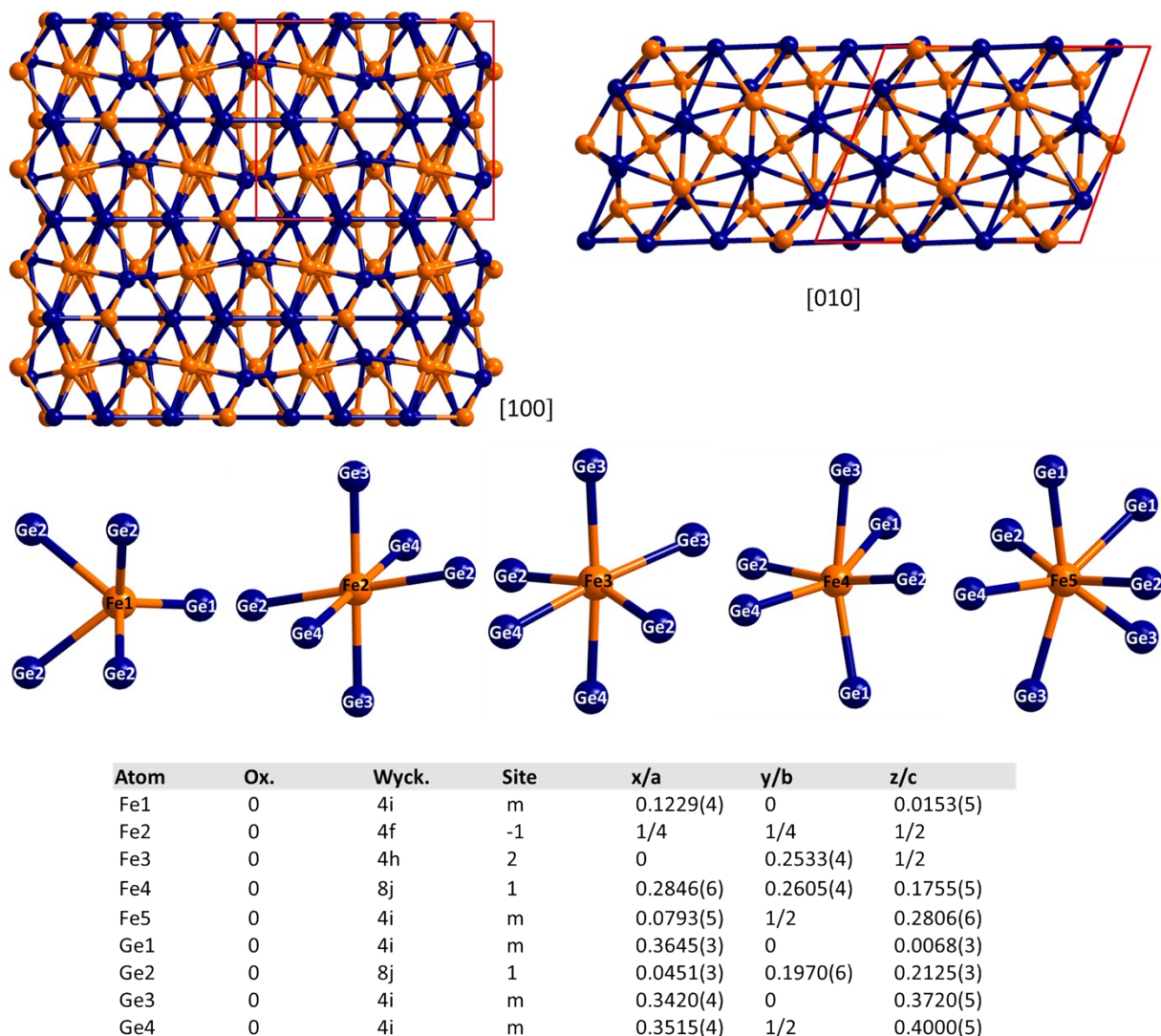
Figure S1. The crystal structure of Fe_6Ge_5 along [100] and [010] as well as the coordination sphere of each Fe atom (colour codes; Fe: orange, Ge: blue).[9,10] Fe_6Ge_5 crystallises in the monoclinic system (space group $C12/m1$; No. 12) with unit cell parameters a = 9.9650 Å, b = 7.8260 Å, c = 7.8010 Å, β = 109.6700°, V = 572.87 Å^3 and Z = 4. The crystal structure can be described as polyhedra of Fe atoms where the Fe(1) is coordinated to five Ge atoms forming a square pyramid while Fe(2), Fe(3), and Fe(4) are linked to six Ge atoms to form distorted octahedra with Ge. Interestingly, Fe(5) is bonded to seven Ge atoms and forms a pentagonal prism. The Table lists the atomic parameters of Fe_6Ge_5.
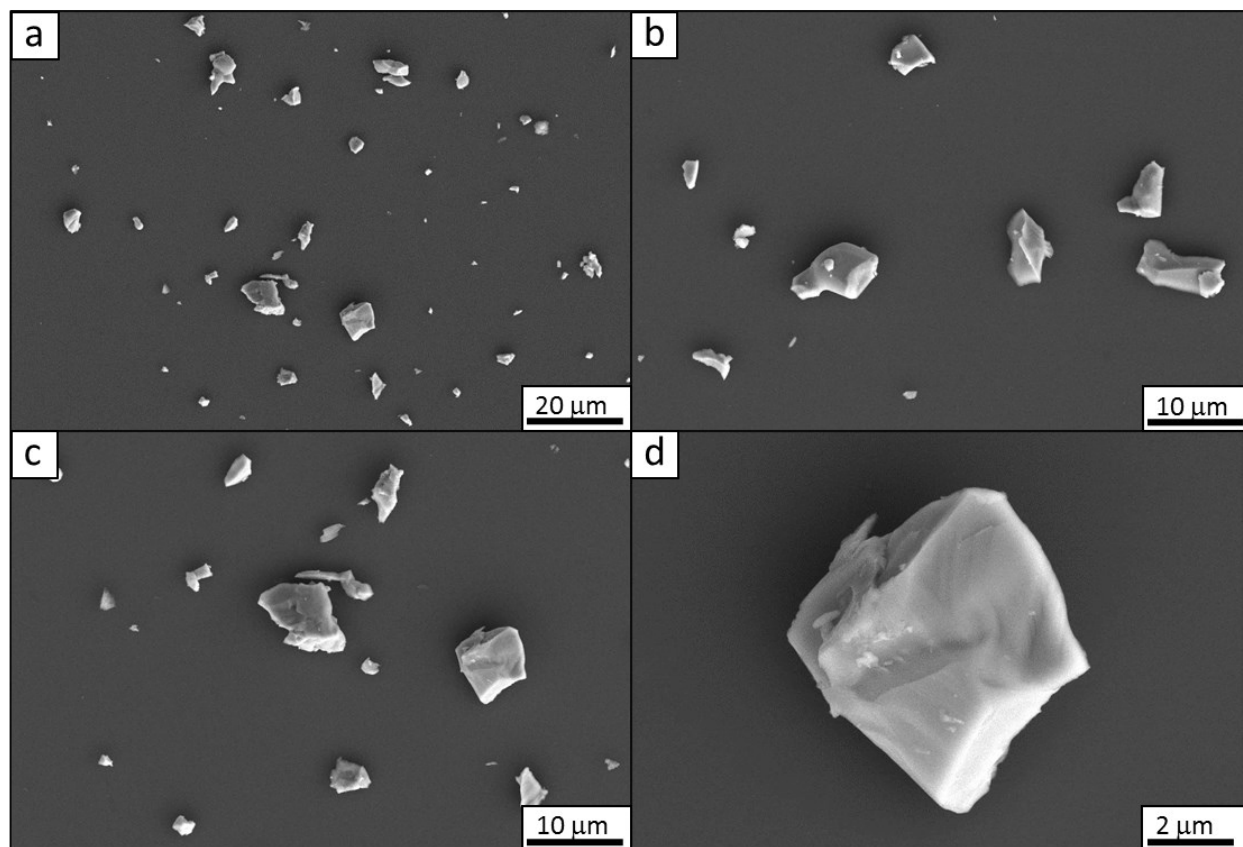
Figure S2. SEM images of the pristine Fe_6Ge_5 powder at different magnifications.
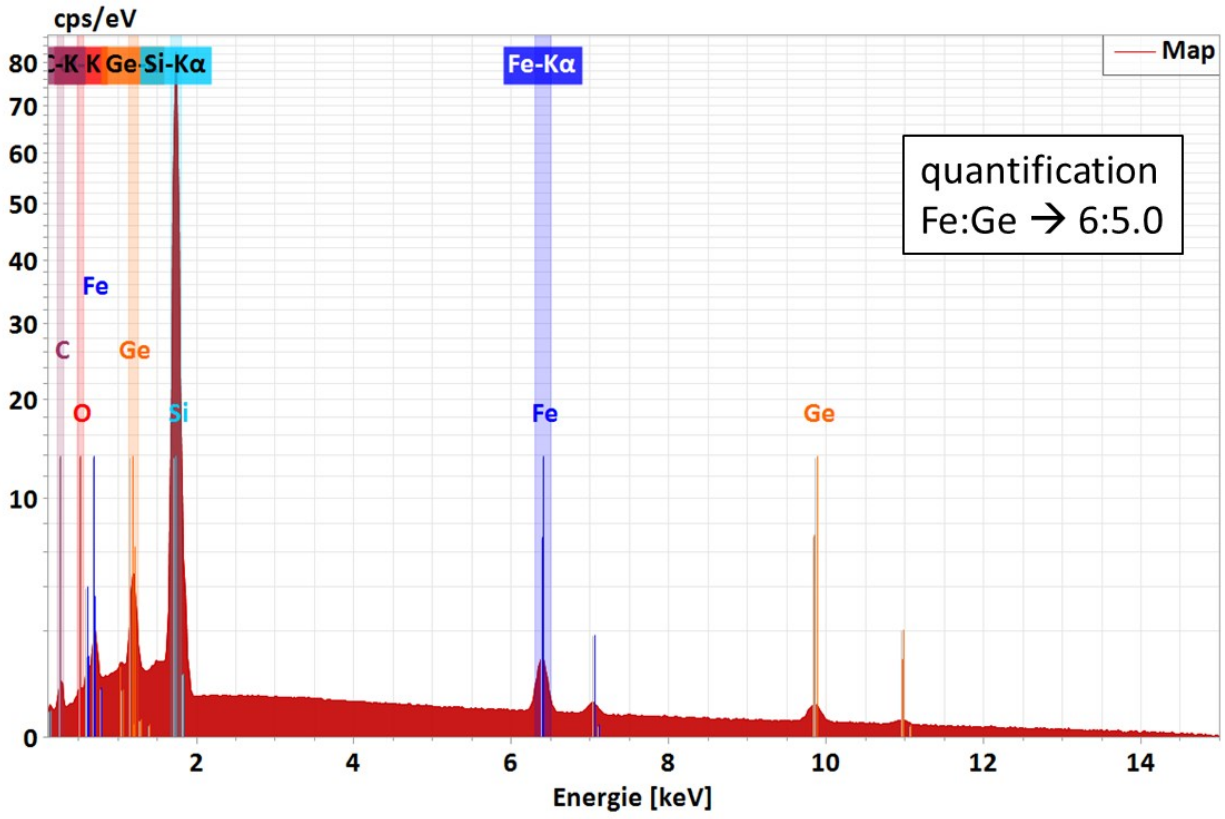
Figure S3. SEM/EDX spectrum of Fe_6Ge_5 of the EDX mapping shown in Fig. 1c of the main text. The presence of the Si peaks arises from the Si wafer support used in SEM.
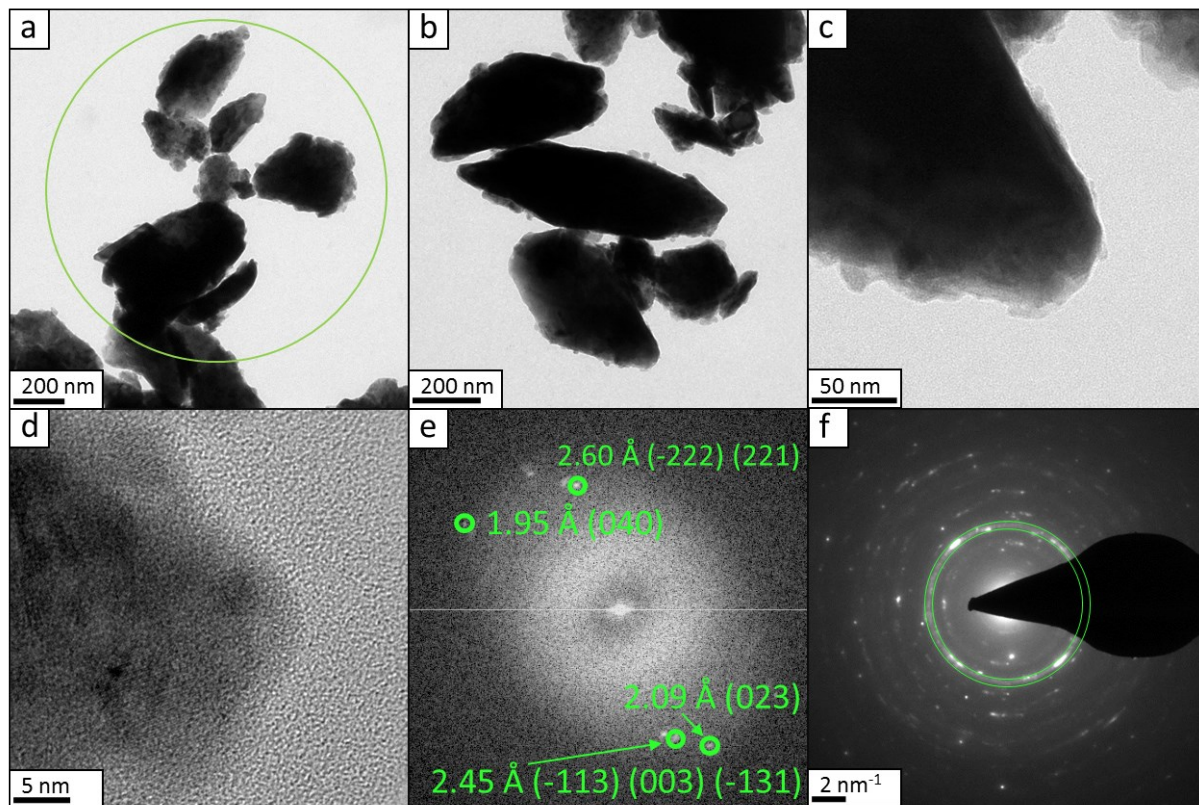
Figure S4. TEM images of mortar ground Fe_6Ge_5 at different magnifications (a-c). Note that the particle size is different to the one observed in the SEM of the pristine powder (see Fig. S2). There are three reasons for that: first, the sample was mortar ground; second, the TEM sample preparation method selects preferably small particles; and third, the TEM of large particles cannot be performed as the electron beam cannot penetrate them. To get a realistic impression of the particle size of the mortar ground and deposited Fe_6Ge_5 particles, the SEM images of the deposited films are suitable (see Fig. S7 and S9). (e) high resolution TEM image of the same sample with its referring fast Fourier transform (FFT). In (e) lattice distances consistent with the crystal structure of Fe_6Ge_5 are marked in green. (f) selected area diffraction pattern (SAED) of the area marked by the green circle in a. Fe_6Ge_5 has a complex unit cell and the reported diffraction file (JCPDS No. 73-1024) contains more than 180 interplane distances in the range of 1 to 6 Å. Hence, for basically every diffraction spot, at least one set of Miller indexes can be found. Characteristic for the Fe_6Ge_5 diffraction pattern is that the five most intense reflections are originating from interplane distances between 1.95 to 2.09 Å. Thus, we have marked this area with two green circles in the SAED pattern f. The most intense reflections of SAED are situated in between these two circles, which is consistent with the pXRD data.
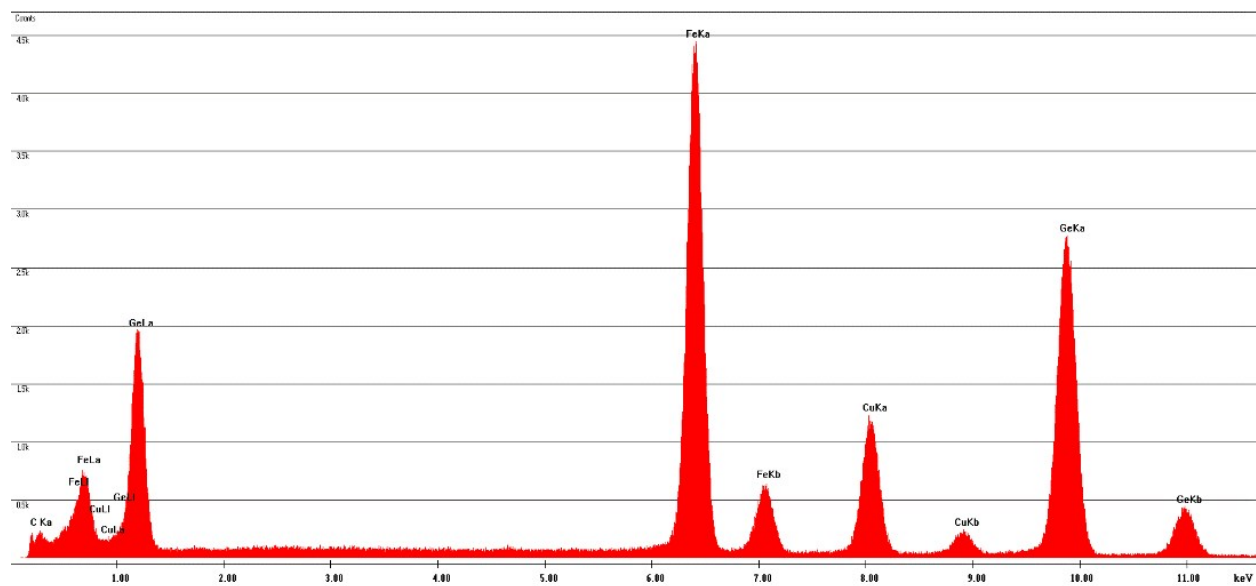
Figure S5. TEM/EDX spectrum of the area marked with a green circle in Fig. S4a. The sample holder was a copper grid with a 2 nm thick carbon film.
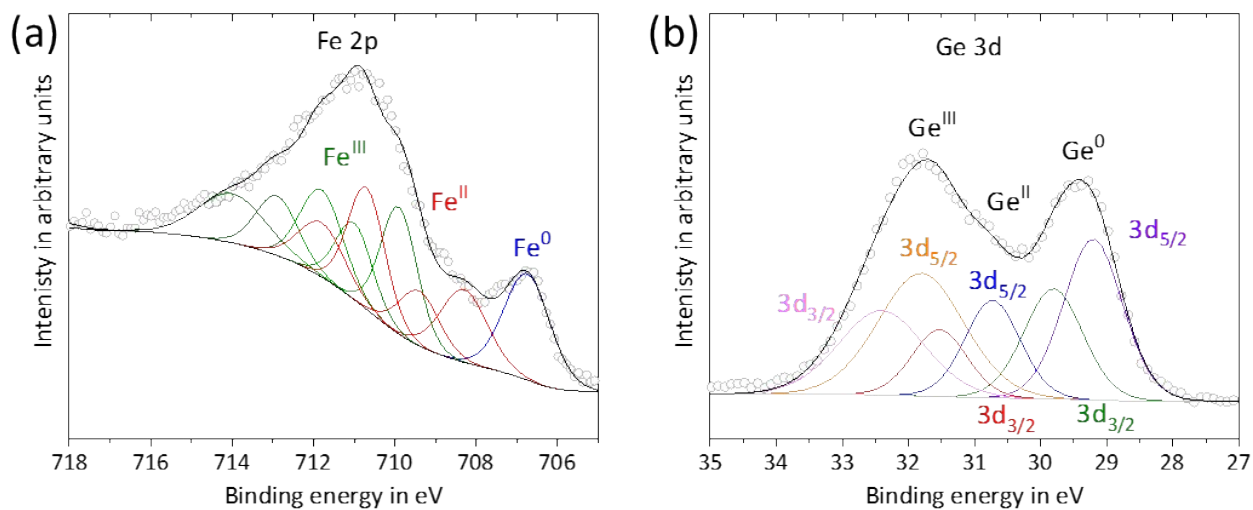
Figure S6. Fe 2p (a) and Ge 3d (b) XPS spectrum of the pristine Fe_6Ge_5 powder.
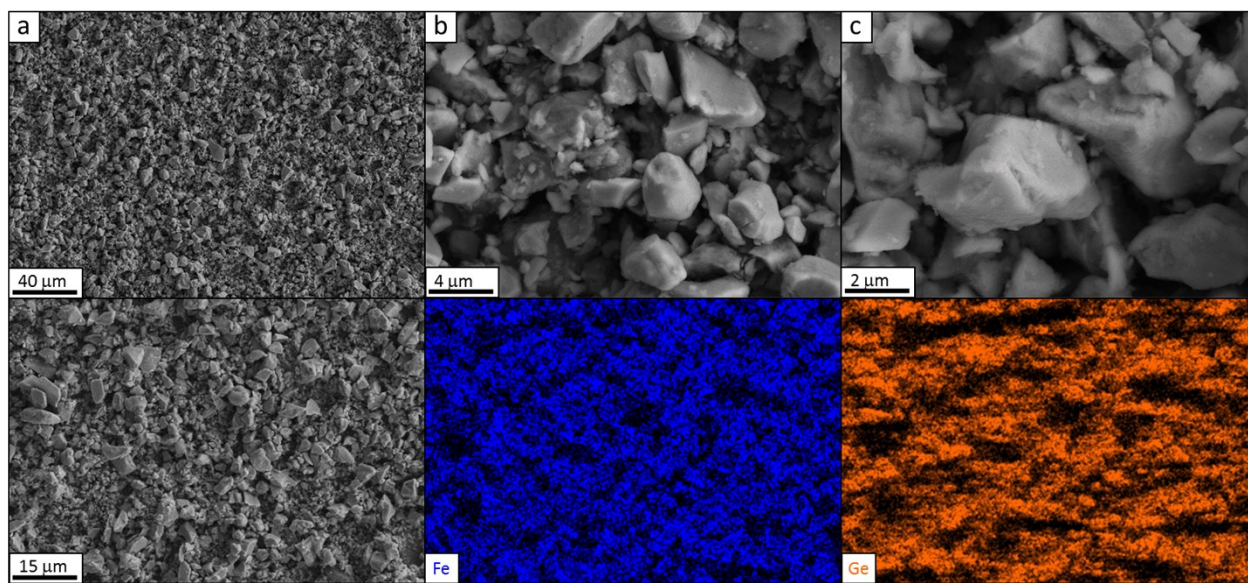
Figure S7. SEM images of Fe_6Ge_5 deposited on FTO (Fe_6Ge_5/FTO, a-c). Bottom: SEM/EDX mapping of Fe_6Ge_5/FTO.
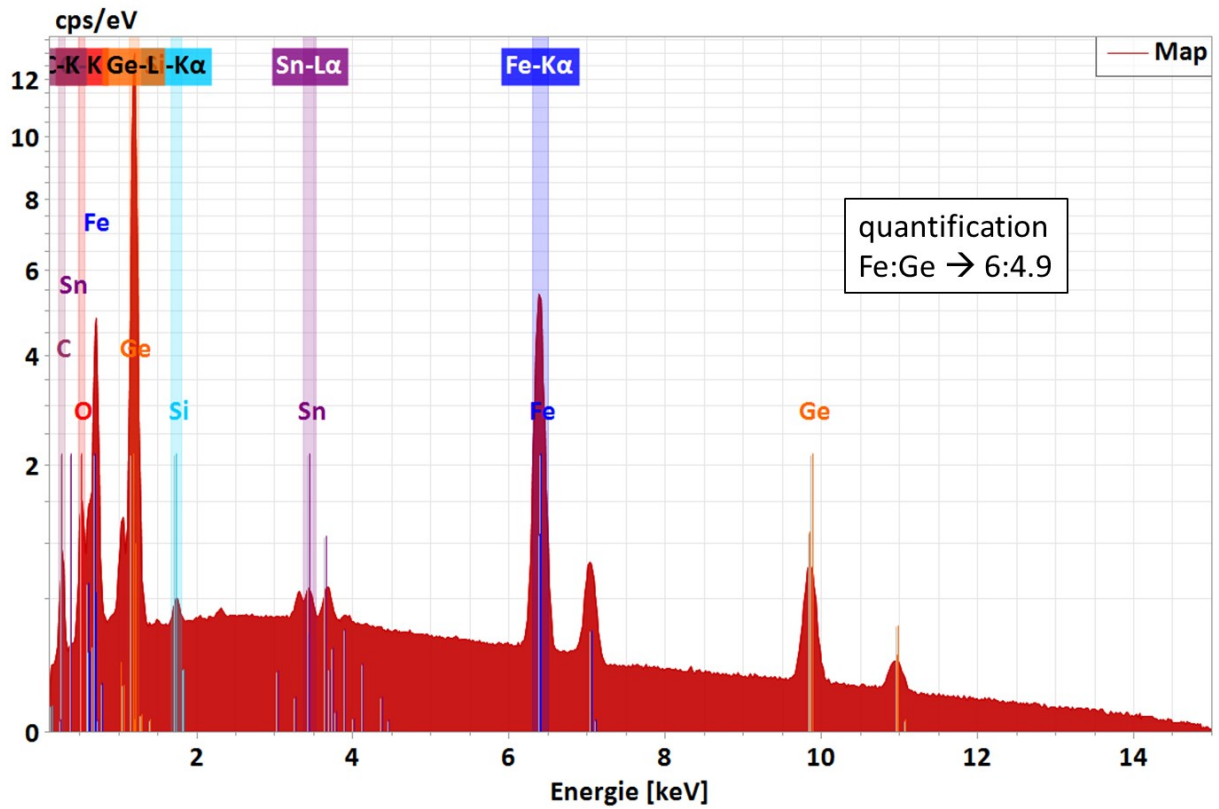
Figure S8. SEM/EDX spectrum of the mapping shown in Fig. S7 bottom. The presence of the Si peaks arises from the Si wafer support used in SEM.
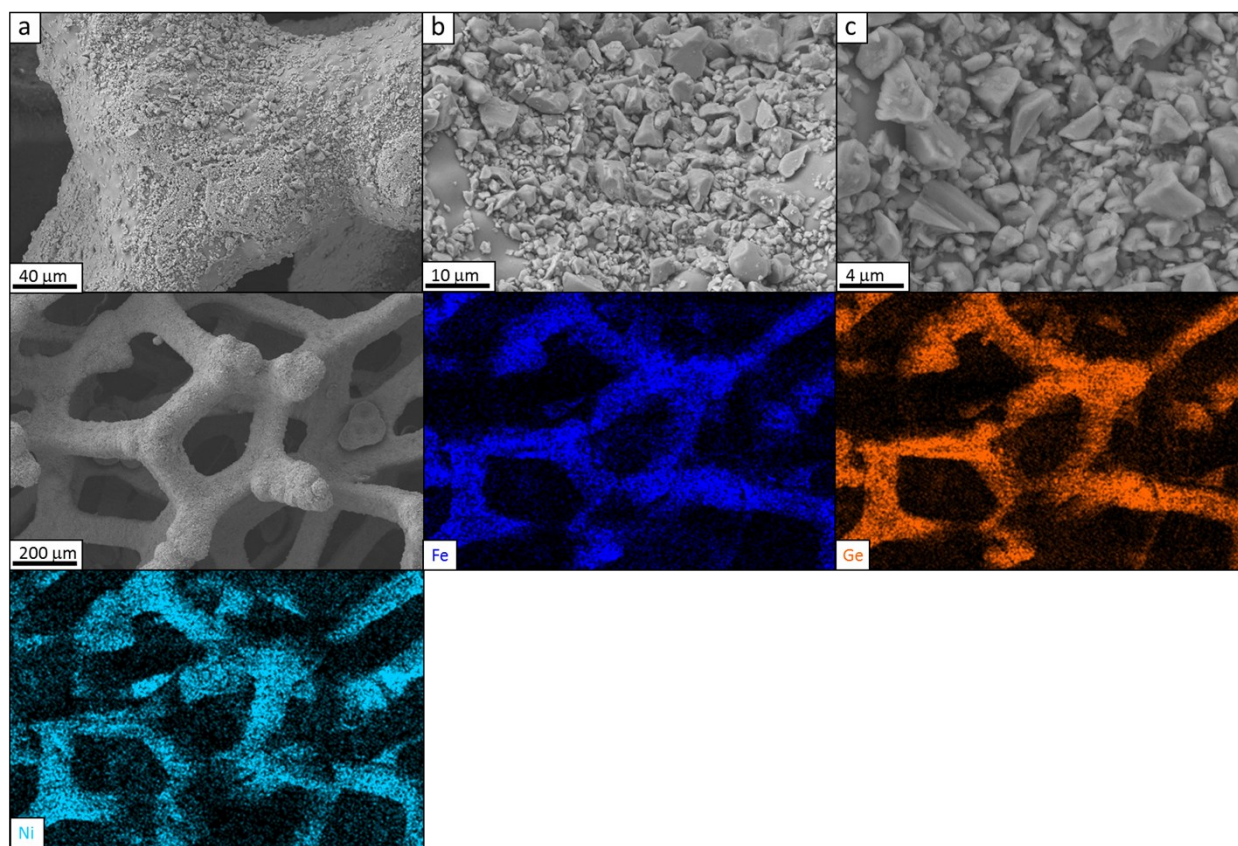
Figure S9. SEM images of Fe_6Ge_5 deposited on NF (Fe_6Ge_5/NF, a-c). The four pictures below show a SEM/EDX mapping of Fe_6Ge_5/NF.
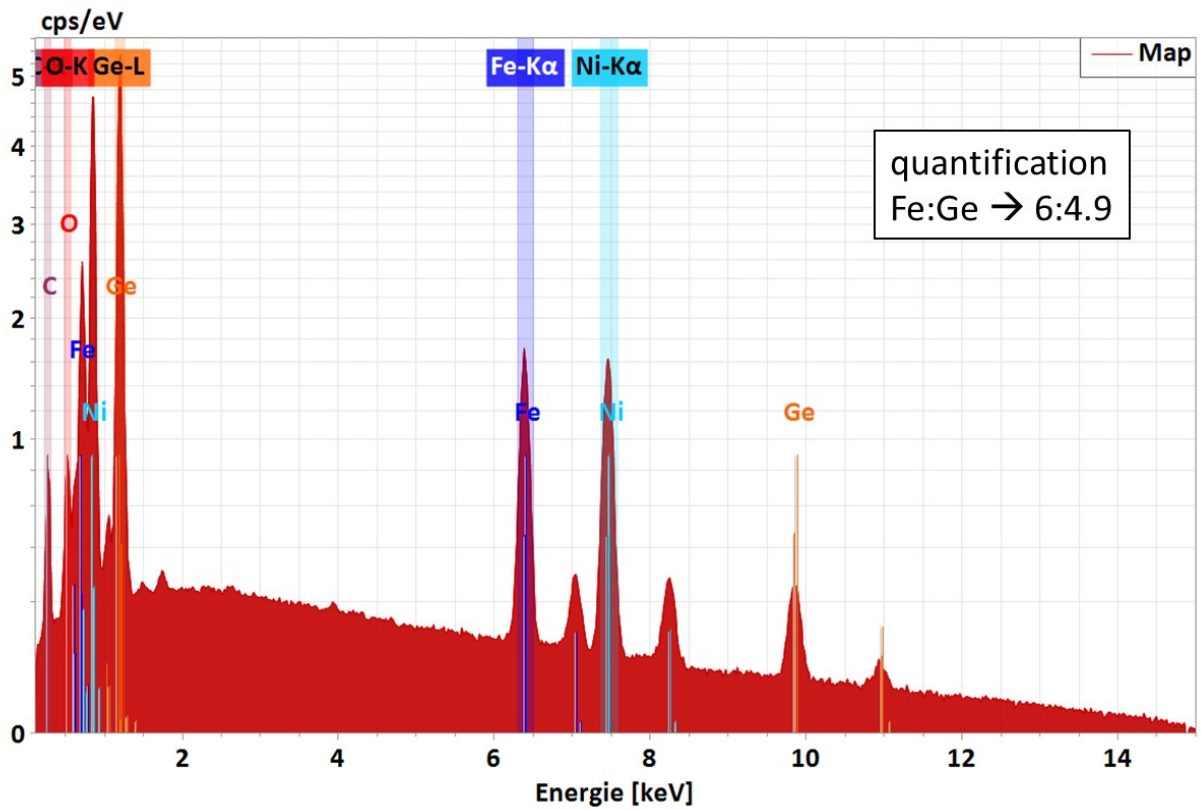
Figure S10. SEM/EDX spectrum of the mapping shown in Fig. S9.
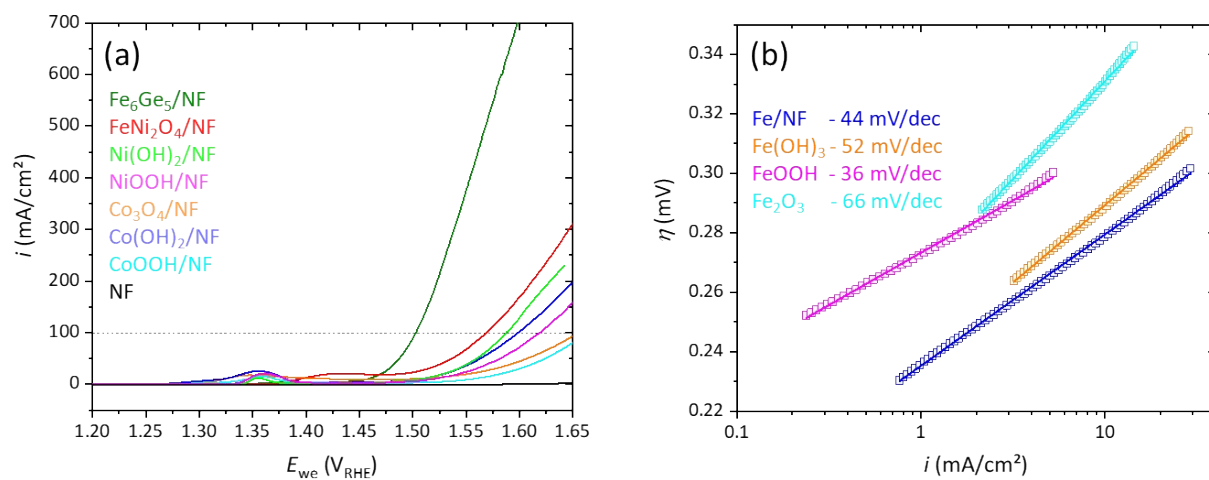
Figure S11. (a) LSVs (1 mV/s) of various reference materials and Fe_6Ge_5 deposited on NF (loading: 1 mg/cm²). (b) Tafel slopes derived from LSVs (1 mV/s) for the Fe containing reference materials.

Table S1. Comparison of water oxidation (η) overpotentials of Fe_6Ge_5 with other established selected non-noble transition metal-based catalysts in aqueous 1 M KOH.

Catalyst	j (mA cm^{-2})	Substrate	Stability (h)	η (mV)	Reference
Fe_6Ge_5	**10**	**FTO**	**1.5**	**420**	**This work**
Fe_6Ge_5	**10**	**NF**	**24**	**221**	**This work**
$LiCo(H_2O)_2[BP_2O_8]\cdot H_2O$	10	FTO	24	293	*Energy Environ. Sci.* 12, 988-99 (2020)
$LiCo(H_2O)_2[BP_2O_8]\cdot H_2O$	10	NF	1752	216	*Energy Environ. Sci.* **13**, 3607-19 (2020)
$CoSeO_3\cdot H_2O$	10	FTO	168	310	*Energy Environ. Sci.* **13**, 3607-19 (2020)
Cu_2FeSnS_4	10	FTO	-	365	*ChemCatChem* **12**, 1161-68, (2020)
Cu_2FeSnS_4	10	NF	28	228	*ChemCatChem* **12**, 1161-68, (2020)
NiFeOOH	10	NiFe	2	240	*ChemSusChem* **12**, 1966-76, (2019)
NiO_x-Fe	10	NF	18	215	*ACS Cent. Sci.* **5**, 558-68, (2019
NiFe LDH	10	NF	13	300	*Nat. Commun.* **5 4477**, (2014)
Fe–O–Ni(OH)$_2$/NF	10	NF	50	185	*J. Mater. Chem. A* **6**, 16810-7, (2018)
$Ni_3Fe_{0.5}V_{0.5}$	10	CFP	60	200	*Nat. Commun.* **9, 1038**, (2018)
NiFe LDH	10	NF	100	184	*Energy Environ. Sci.* **12**, 572-81, (2019)
FeCoW-oxyhydroxide	10	Au	550	223	*Science* **352**, 333-7, (2016)
NiFe LDH	10	GC	1	210	*ACS Nano* **9**, 1977-84, (2015)
$Co_4Fe(OH)_x$	10	GC	3	295	*J. Mater. Chem. A* **5**, 1078-84, (2017)
$ZnCo_2O_4$	10	FTO	-	390	*J. Phys. Chem. Lett* **5**, 2370-4, (2014)
$CoO-MoO_2$	10	NF	1	270	*Nanoscale* **7**, 16704-14, (2015)
$CoS_{4.6}O_{0.6}$	10	GC	2	290	*Angew. Chem. Int. Ed.* **56**, 4858-61, (2017)
FeOOH/Co/FeOOH	10	NF	50	245	*Angew, Chem. Int. Ed.* **55**, 3694-8, (2016)
Fe_7S_8	10	GC	24	270	*ACS Cent. Sci.* **3**, 1221-7, (2017)
Co_4N	10	CC	12	257	*Angew, Chem. -Int. Ed.* **54**, 14710-4, (2015)
Ni_2P	10	NF	12	240	*ACS Catal.* **7**, 103-9, (2017)
$Ni_{12}P_5$	10	NF	12	260	*ACS Catal.* **7**, 103-9, (2017)
MoO_2	10	NF	24	250	*Adv. Mater.* **28**, 3785-90, (2016)
NiFe LDH	10	HOPG	5	260	*J. Am. Chem. Soc.* **136**, 13118-21, (2014)
Ni_3S_2	10	NF	200	260	*J. Am. Chem. Soc.* **137**, 14023-6, (2015)
CoFeP	10	NF	10	244	*ACS Appl. Mater. Interfaces* **9**, 362-70, (2017)
NiFe-LDH	10	NF	3	240	*Electrochimi. Acta* **225**, 303-9, (2017)
FeP	10	NF	15	227	*Chem. Sci.* **9**, 8590–7, (2018)
CoP amorphous	10	NF	24	284	*J. Mater. Chem. A* **7**, 15749-56, (2019)
$CoSn_2$	10	NF	14	230	*Angew. Chem. -Int. Ed.* **57**, 15237-42, (2018)
$Co_3(OH)_2(HPO_4)_2$	10	FTO	24	292	*Adv. Funct. Mater.* **29**, (2019)
CoP	10	FTO	24	360	*J. Mater. Chem. A* **7**, 15749-56, (2019)
Ni_2P	10	FTO	16	330	*ACS Catal.* **7**, 103-9, (2017)
$Ni_{12}P_5$	10	FTO	16	295	*ACS Catal.* **7**, 103-9, (2017)
$FeNiO_xH_y$	10	NF	50	206	*ChemSusChem* **11**, 1761-7, (2018)
$CuO@NiFeOH_x$	10	Cu	16	230	*ChemSusChem* **11**, 1761-7, (2018)
NiFe-LDH	10	NW	1.5	300	*ACS Appl. Energ. Mater.* **2**, 5465-5471, (2019)

GC = glassy carbon, CFP = carbon fiber paper, Au = gold, CC =carbon cloth, FTO = fluorine doped tin oxide, HOPG = highly-ordered pyrolytic graphite, NF = nickel foam, CW= carbon wire, NW = nickel wire
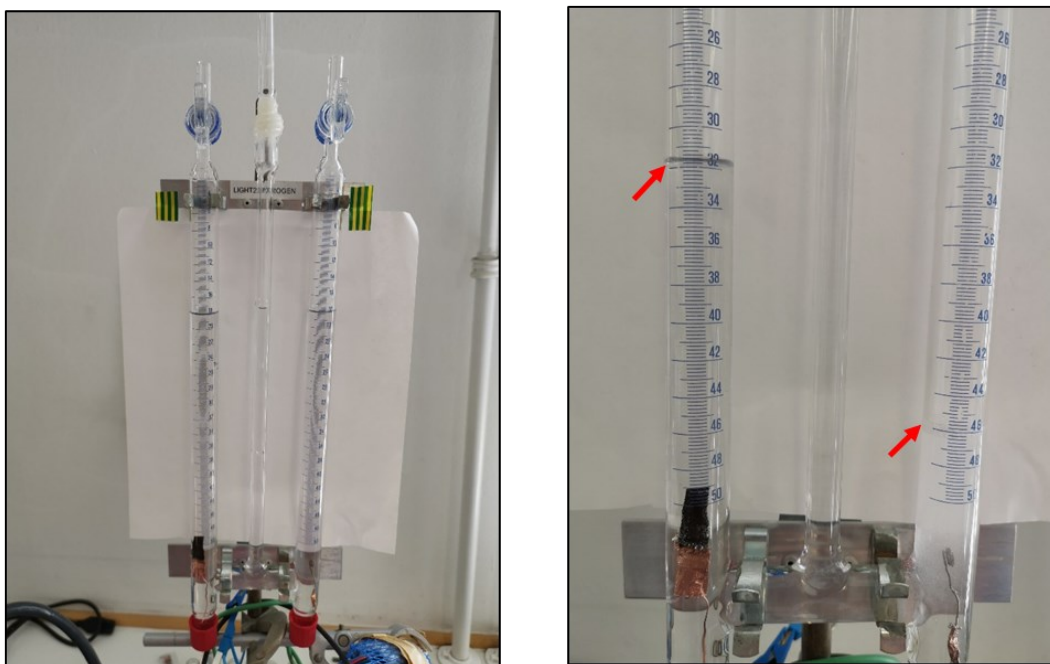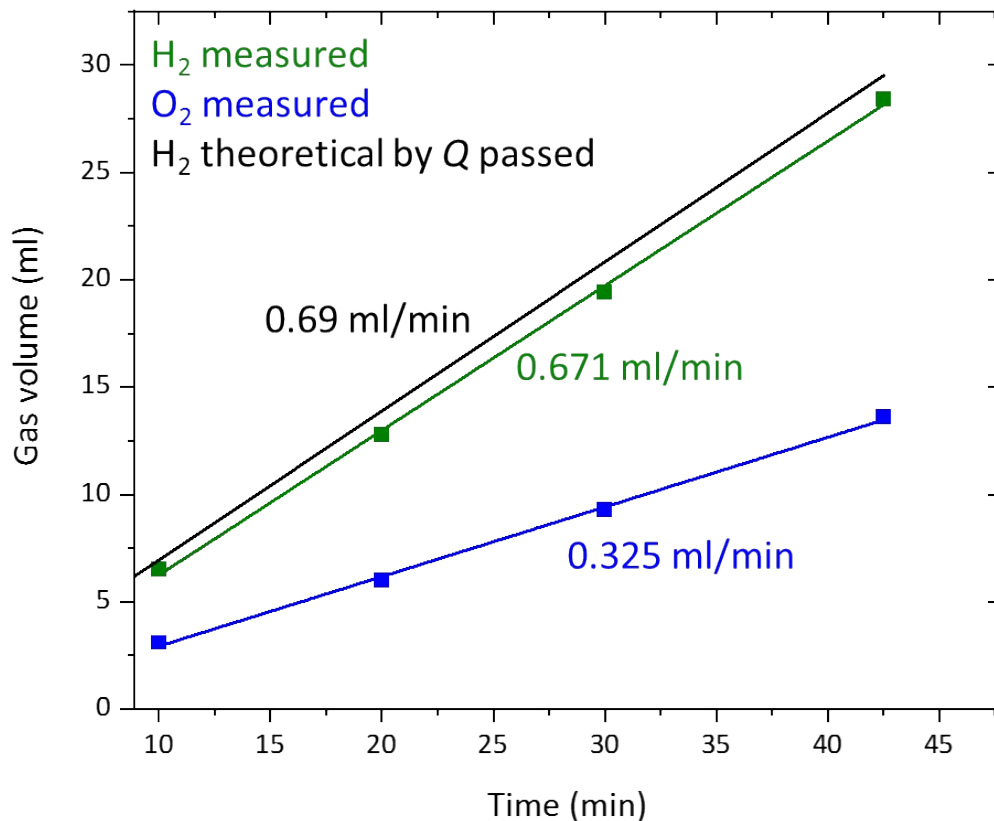
Figure S12. Top: Plot of the FE measurement of Fe_6Ge_5/NF. Bottom: Pictures of the experimental setup at the beginning (left) and the end (right) of the measurements. The OER FE was determined to be 97% based on the H_2 to O_2 ratio and 94% based on the charge passed compared to the amount of evolved O_2. Further experimental details can be found in section Faradaic efficiency (FE) at the beginning of the ESI.
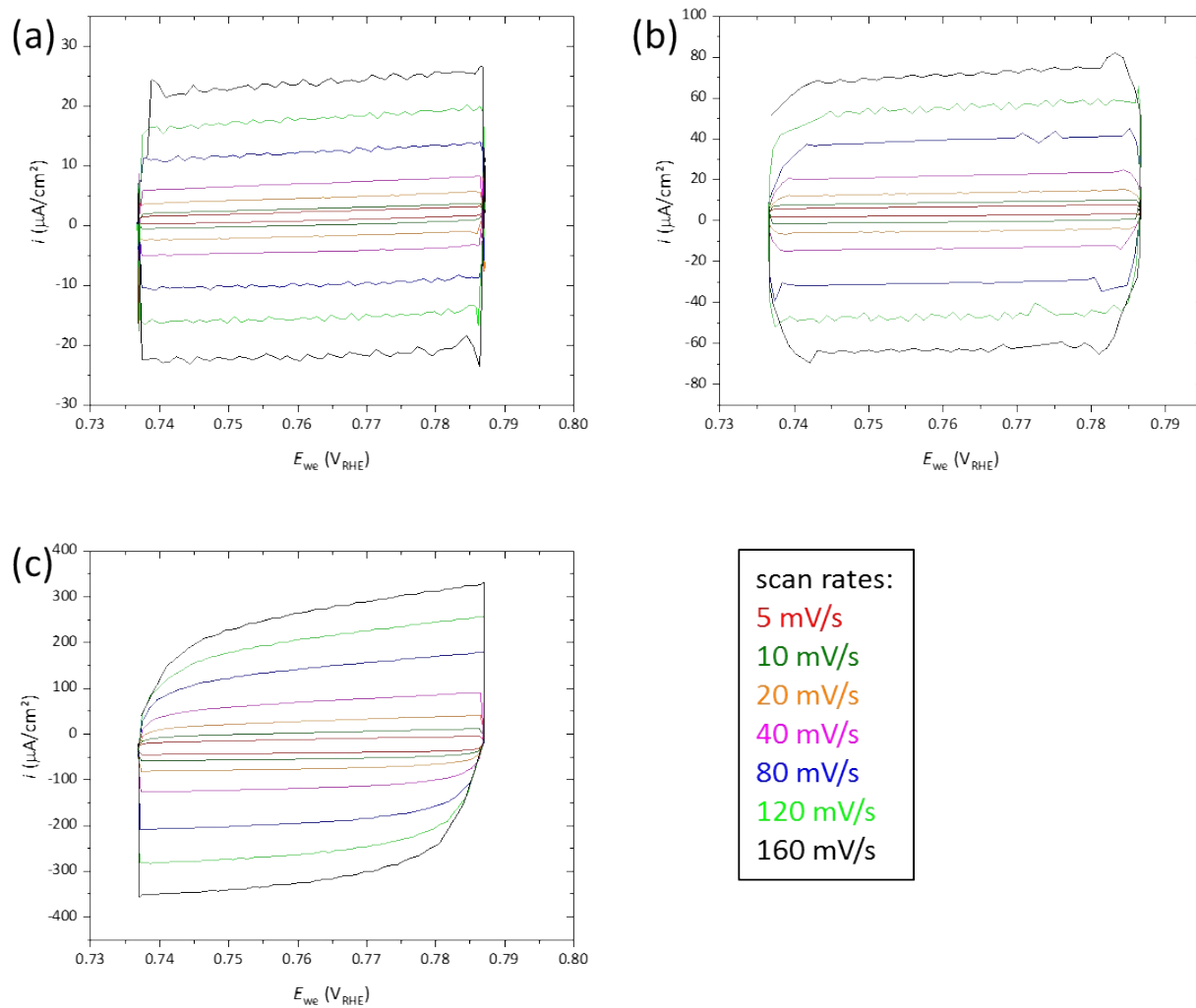
Figure S13. Cyclic voltammograms in a region without apparent Faradaic process at different scan rates for the determination of the C_{dl} of pristine NF (a), Fe_6Ge_5/NF before any OER measurement (b), and Fe_6Ge_5/NF after 25 h at η = 280 mV (c).
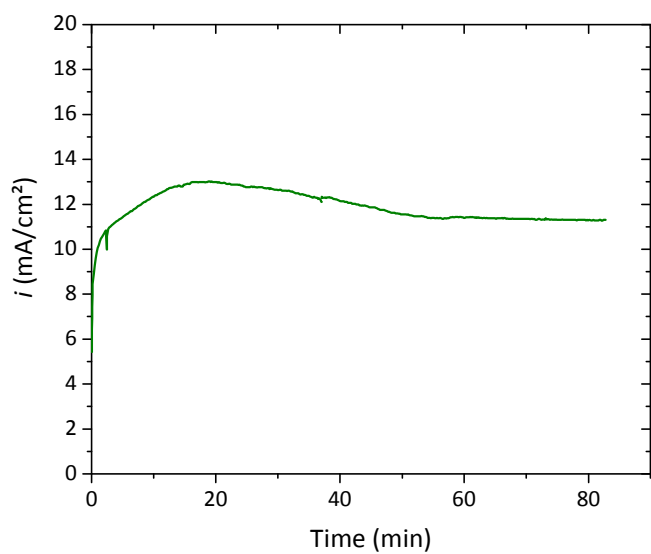
Figure S14. CA measurement of Fe_6Ge_5/FTO at η = 430 mV.
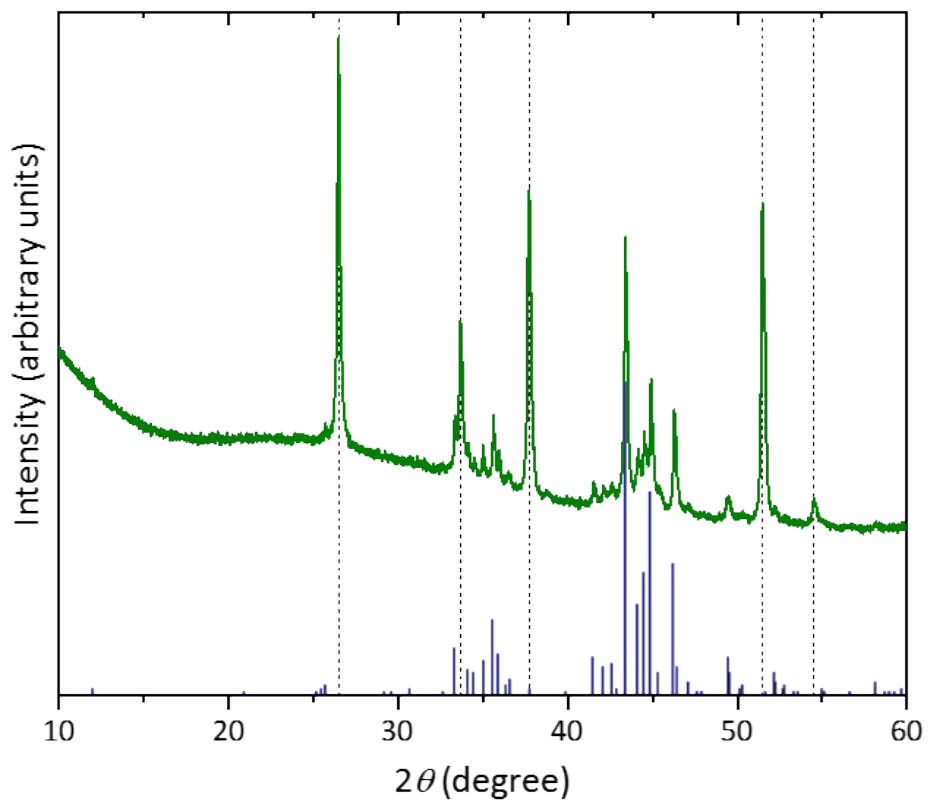
Figure S15. pXRD of a Fe_6Ge_5/FTO sample after 1 h OER at η = 430 mV. The blue bars indicate the position and intensity of the original Fe_6Ge_5 phase (JCPDS No. 73-1024). The dashed black lines indicate the position of the reflections that originate from the FTO substrate.
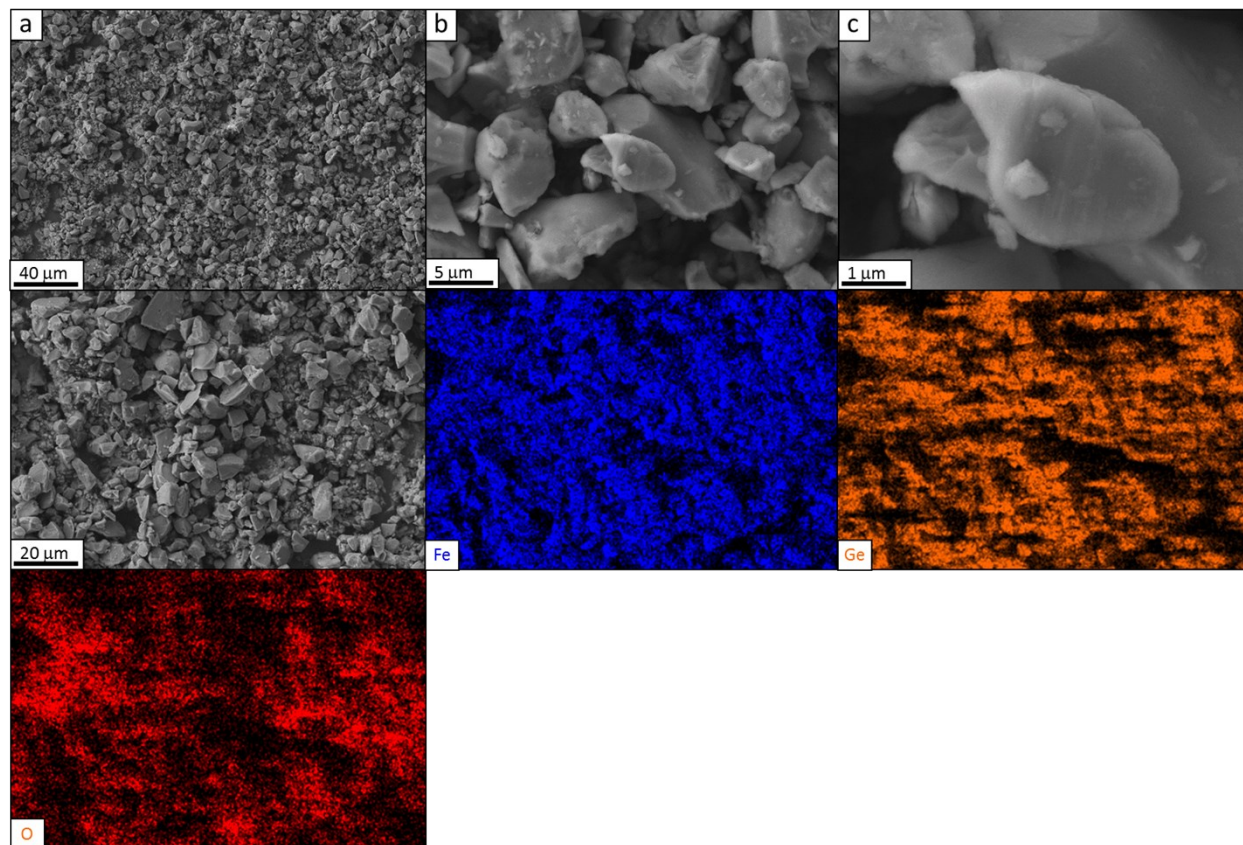
Figure S16. SEM images of Fe$_6$Ge$_5$/FTO after 1 h OER at η = 430 mV (a-c). The four pictures below show a SEM/EDX mapping of the same sample.
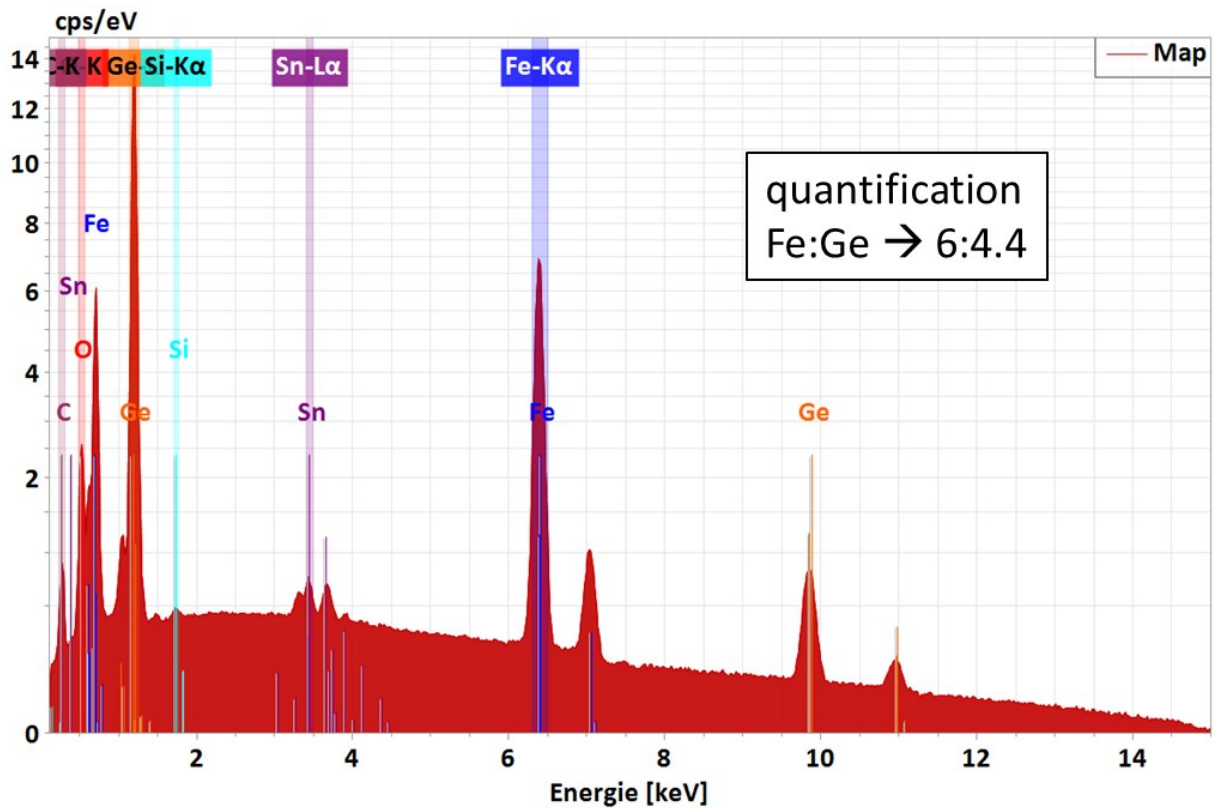
Figure S17. SEM/EDX spectrum of the mapping shown in Fig. S16. The presence of the Si peaks arises from the Si wafer support used in SEM.
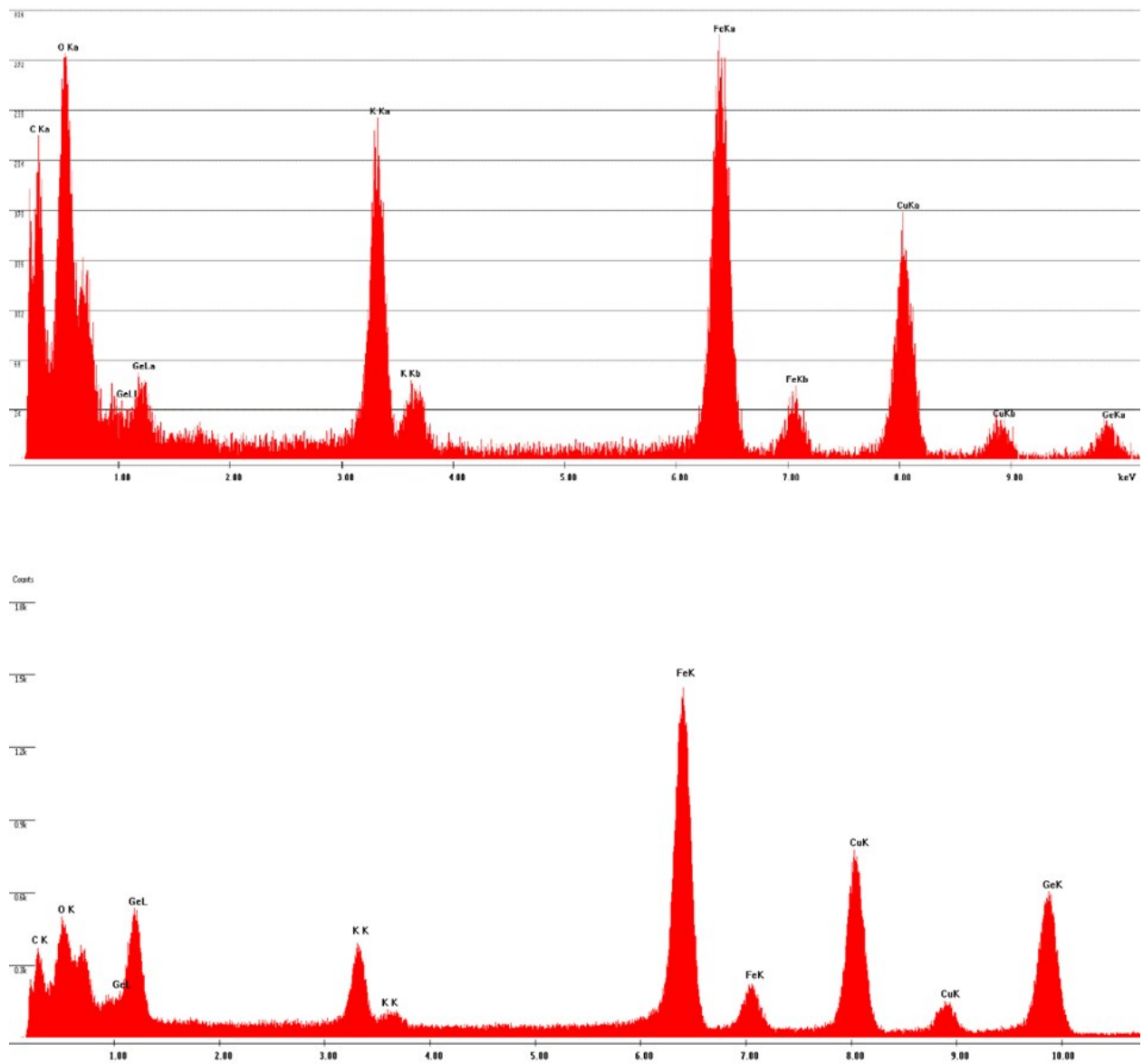
Figure S18. TEM/EDX spectrum of area 1 in Fig. 3a (top) and of area 2 in Fig. 3a (bottom). The EDX quantifications of these two spectra are shown in Fig. 3c and d. The sample holder was a copper grid with a 2 nm thick carbon film**.**
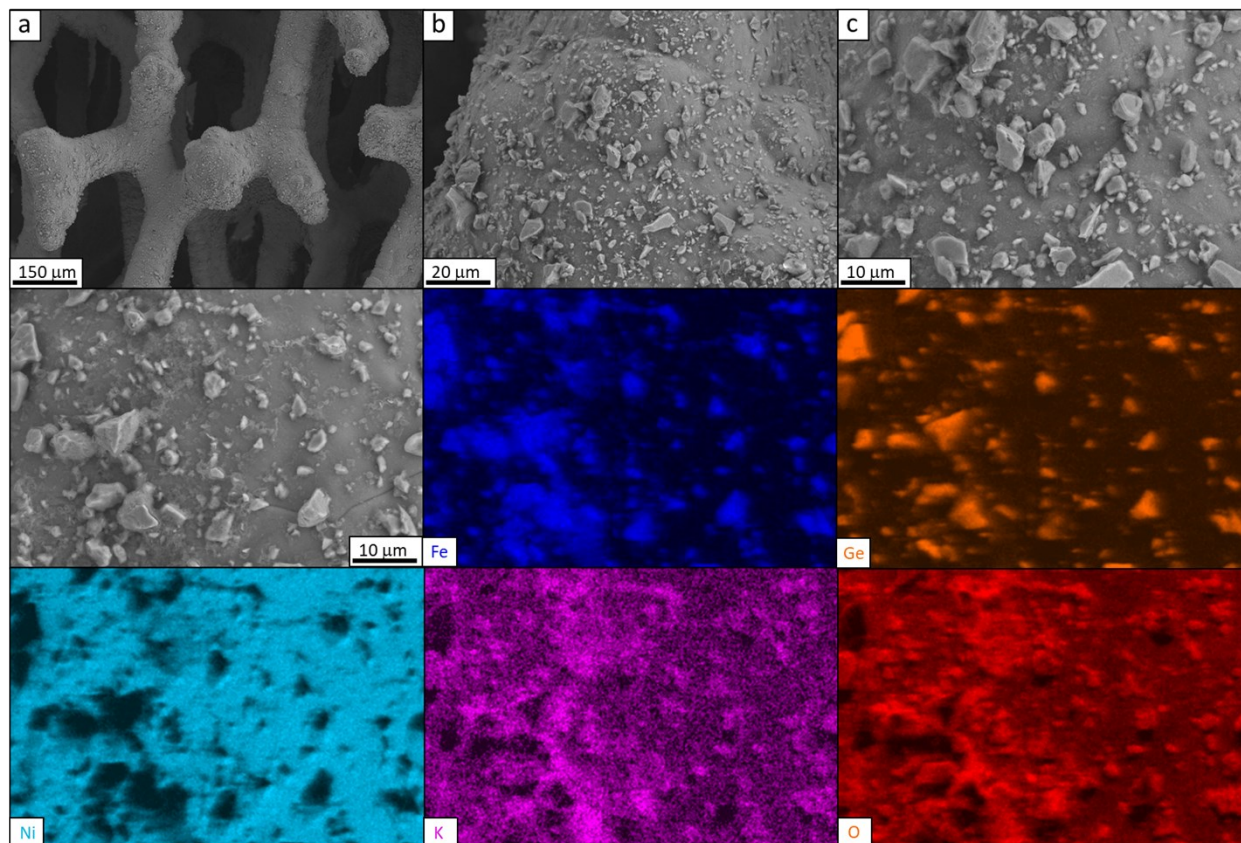
Figure S19. SEM images of Fe$_6$Ge$_5$/NF after 25 h OER at η = 280 mV (a-c). The six pictures below show a SEM/EDX mapping of the same sample.
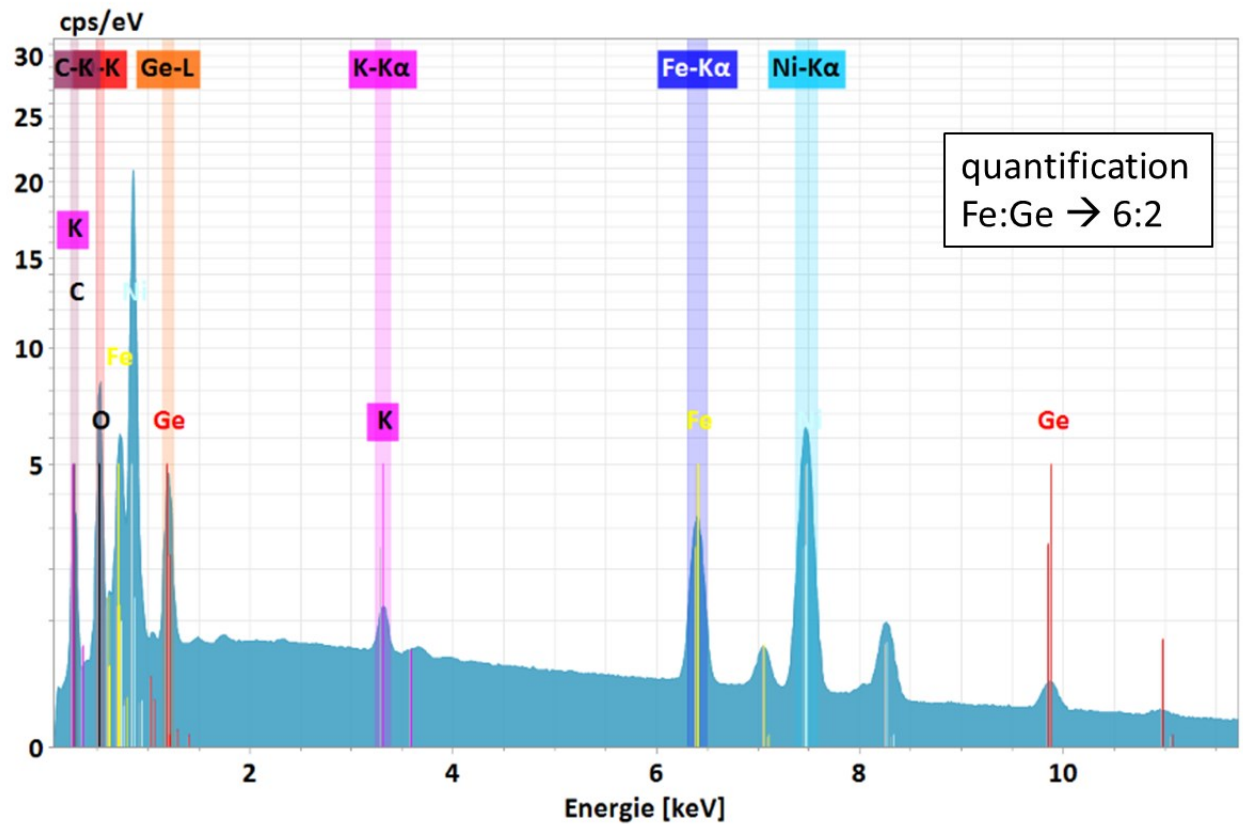
Figure S20. SEM/EDX spectrum of the mapping shown in Fig. S19.
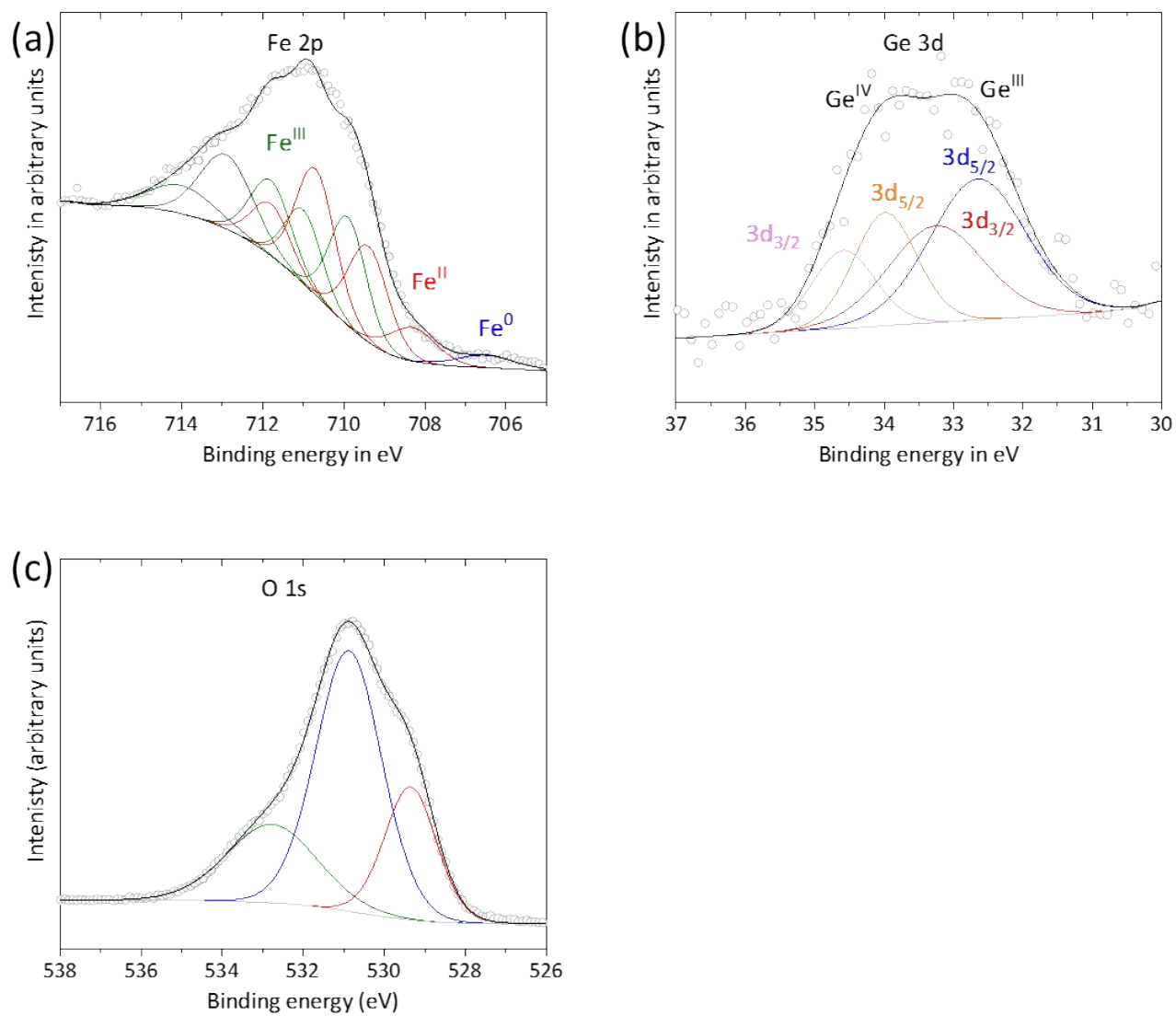
Figure S21. Fe 2p (a), Ge 3d (b), and O 1s XPS spectrum of Fe_6Ge_5/NF after 25 h OER at η = 280 mV.

References

1   B. Chakraborty, R. Beltrán-Suito, J. N. Hausmann, S. Garai, M. Driess and P. W. Menezes, *Adv. Energy Mater.*, 2020, **10**, 2001377.

2   J. N. Hausmann, S. Mebs, K. Laun, I. Zebger, H. Dau, P. W. Menezes and M. Driess, *Energy Environ. Sci.*, 2020, **13**, 3607–3619.

3   N. Koura, T. Tsukamoto, HiromasaShoji and T. Hotta, *Jpn. J. Appl. Phys.*, 1995, **34**, 1643–1647.

4   P. W. Menezes, C. Panda, S. Loos, F. Bunschei-Bruns, C. Walter, M. Schwarze, X. Deng, H. Dau and M. Driess, *Energy Environ. Sci.*, 2018, **11**, 1287–1298.

5   P. W. Menezes, A. Indra, I. Zaharieva, C. Walter, S. Loos, S. Hoffmann, R. Schlögl, H. Dau and M. Driess, *Energy Environ. Sci.*, 2019, **12**, 988–999.

6   C. Panda, P. W. Menezes, S. Yao, J. Schmidt, C. Walter, J. N. Hausmann and M. Driess, *J. Am. Chem. Soc.*, 2019, **141**, 13306–13310.

7   C. C. L. McCrory, S. Jung, J. C. Peters and T. F. Jaramillo, *J. Am. Chem. Soc.*, 2013, **135**, 16977–16987.

8   C. C. L. McCrory, S. Jung, I. M. Ferrer, S. M. Chatman, J. C. Peters and T. F. Jaramillo, *J. Am. Chem. Soc.*, 2015, **137**, 4347–4357.

9   A. Larsson, S. Furuseth and R. Withers, *J. Solid State Chem.*, 1998, **141**, 199–204.

10   B. Malaman, M. J. Phillippe, B. Roques, A. Courtois and J. Protas, *Acta Crystallogr. Sect. B Struct. Crystallogr. Cryst. Chem.*, 1974, **30**, 2081–2087.